Electrical conductivity model for reactive porous media under partially saturated conditions with hysteresis effects

Mariangeles Soldi, Flore Rembert, Luis Guarracino, Damien Jougnot

Electrical conductivity model for reactive porous media under partially saturated conditions with hysteresis effects

M. Soldi[1,3*], F. Rembert[2], L. Guarracino[1] and D. Jougnot[3]
[1]Facultad de Ciencias Astronómicas y Geofísicas, Universidad Nacional de La Plata, Consejo Nacional de Investigaciones Científicas y Técnicas, La Plata, Argentina
[2]Univ. Orléans, CNRS, BRGM, ISTO, UMR 7327, F-45071 Orléans, France
[3]Sorbonne Université, CNRS, EPHE, UMR 7619 METIS, 75005, Paris, France
*E-mail: msoldi@fcaglp.unlp.edu.ar

This paper has been published in Advances in Water Resources:
Soldi, M., Rembert, F., Guarracino, L., Jougnot, D. (2024) Electrical conductivity model for reactive porous media under partially saturated conditions with hysteresis effects. Advances in Water Resources. Volume 193, 2024, 104815, ISSN 0309-1708, https://doi.org/10.1016/j.advwatres.2024.104815.

Abstract

The electrical conductivity of a porous medium is strongly controlled by the structure of the medium at the microscale as the pore configuration governs the distribution of the conductive fluid. The pore structure thus plays a key role since different geometries translate in variations of the fluid distribution, causing different behaviours measurable at the macroscale. In this study, we present a new physically-based analytical model derived under the assumption that the pore structure can be represented by a bundle of tortuous capillary tubes with periodic variations of their radius and a fractal distribution of pore sizes. By upscaling the microscale properties of the porous medium, we obtain expressions to estimate the total and relative electrical conductivity. The proposed pore geometry allows us to include the hysteresis phenomenon in the electrical conductivity estimates. The variations on these estimates caused by pore structure changes due to reactive processes are accounted by assuming a uniform dissolution of the pores. Under this hypothesis, we describe the evolution of the electrical conductivity during reactive processes. The expressions of the proposed model have been tested with published data from different soil textures, showing a satisfactory agreement with the experimental data. Hysteretic behavior and mineral dissolution are also successfully addressed. By including hysteresis and mineral dissolution/precipitation in the estimates of the electrical conductivity, this new analytical model presents an improvement as it relates those macroscopic physical phenomena to its origins at the microscale. This opens up exciting possibilities for studies involving electrical conductivity measurements to monitor water movement, and hysteretic and reactive processes in porous media.

Highlights

- New electrical conductivity model for partially saturated reactive porous media.

- Pore structure composed of capillaries with periodic reductions of their radii.
- Variations in pore structure significantly influence the electrical conductivity.
- Hysteretic behavior is included from geometrical effects, pore radii reductions.
- Geometrical impact on the pores due to mineral dissolution is successfully described.

Keywords: Electrical conductivity, Unsaturated flow, Vadose zone, Fractal distribution, Reactive porous media

1 Introduction

The water content and dynamics in geological media are largely controlled by their petrophysical properties (such as permeability and porosity) which often exhibit a high degree of spatial variability due to the irregularities of the pore space structure. Knowledge of these properties is important to understand flow and transport processes as they control the movement and storage of fluids. This fact is highlighted for porous media containing carbonates, since dissolution and precipitation processes can drastically change the size and shape of the pore spaces and the degree of their interconnection (e.g., Noiriel et al., 2004; Leger and Luquot, 2021). Therefore, understanding better the effect of pore geometry at the microscale is a key to describe and predict petrophysical and transport properties at the macroscale.

During the last two decades, the use of geophysical methods to non-invasively characterize hydrological processes has been extensively developed (e.g., Binley et al., 2015; Hermans et al., 2023; Loiseau et al., 2023). Among the geophysical methods, the electrical and electromagnetic methods are very useful since they can provide quantitative information on the structure, water content, or fluid composition of the porous media through the measurement of electrical conductivity. Electrical resistivity tomography (ERT), induced polarization (IP), and electromagnetic induction (EMI) are some of the hydrogeophysical methods that have increasingly been used to monitor flow and transport quantitatively (e.g., Revil et al., 2012; Binley and Slater, 2020). Among many other applications of these methods related to groundwater in porous media, it can be mentioned the application of ERT to monitor critical saturated conditions for landslide occurrence (e.g., Olabode et al., 2020; Wicki and Hauck, 2022), the use of IP to describe contaminant plumes and to monitor their remediation (e.g., Deceuster and Kaufmann, 2012; Schwartz and Furman, 2012), or the capability of EMI to detect and monitor groundwater flow (e.g., Wilson et al., 2002; Zhu et al., 2010; Doolittle and Brevik, 2014).

The electrical conductivity σ (S m^{-1}) of the porous medium is one of the petrophysical properties of interest measured with the electrical methods and electromagnetic methods. Many models exist to express the electrical conductivity of a water-saturated porous media (for a review, see Glover (2015) and Schön (2015)). Among the most simple ones, the pore space can be seen as an electrical circuit in parallel, where σ is linked to the electrical currents that arise when charge carriers (i.e., ions) flow through the media and

can be expressed as:

$$\sigma = \frac{\sigma_w}{F} + \sigma_s \tag{1}$$

where σ_w (S m^{-1}) is the electrical conductivity of the fluid, F (no units) the formation factor and σ_s (S m^{-1}) the surface conductivity. This model was first introduced by Patnode and Wyllie (1950) who discovered that surface conductivity σ_s cannot always be neglected in reservoir rocks. The first term in Eq. (1) corresponds to the contribution from the electrical conduction in the liquid phase (i.e., electrolyte) whereas the second term is the contribution due to the electrical conduction in the liquid–solid interface, the so-called electrical double layer (EDL, e.g., Hunter, 1981; Leroy and Revil, 2004). The electrical conductivity of the electrolyte σ_w has a magnitude that depends on its chemical composition and the ionic concentrations (e.g., Glover, 2015). Experimental and theoretical works, e.g., the three-resistor model (Wyllie and Southwick, 1954; Lévy et al., 2018), the BHS (Bruggeman-Hanai-Sen) model (Sen et al., 1981), and the recent models of (Qi and Wu, 2022, 2024), have shown that the surface conductivity σ_s depends on the water and the EDL electrical conductivities. However, when the surface conductivity σ_s can be neglected, that is when the electrolytic conduction is much larger than the surface one, the electrical conductivity σ is controlled mainly by the pore space geometry in which the charge carriers (i.e., usually ions) can move it. That is the porous medium connectivity and the size and shape of the pores (e.g. Olsen, 2011; Revil, 2013b; Jougnot et al., 2018). The dependency of the porous medium electrical conductivity to its microstructure and the electrolyte conductivity is taken into account through the formation factor, a quantitative proxy for the medium geometry. Petrophysical models aim to establish an expression for the formation factor based on pore structure parameters. Among the existing approaches, models capturing the true pore space topology play a major role when considering the partially saturated conditions. To identify physically-based structural parameters defining the formation factor, several studies have analyzed the effect of pore structure in electrical properties directly related to the electrical conductivity. Müller-Huber et al. (2015) examined the effect of changes in the pore radius on the electrical conductivity. They studied a straight pore channel whose radius increases exponentially between its two extremes showing that pore geometry has a strong effect on the electrical conductivity. For carbonate rocks, Regnet et al. (2019) analyzed the influence of microstructural patterns on petrophysical properties (electrical conductivity, porosity, and permeability). They emphasized the importance of pore space to estimate these properties through many parameters such as pore size and shape, grain contacts or cracks, pore network connectivity, and mineralogy. Rembert et al. (2020) derived a model that estimates the electrical conductivity and the formation factor as a function of both tortuosity and constrictivity of the pore structure. They observed that the constrictivty follows a monotonous variation either during dissolution or precipitation processes.

Among the models to predict the electrical conductivity of porous media for both saturated and partially saturated conditions, the most widely used is the one proposed by Archie (1942). Assuming negligible surface conductivity, this empirical model provides a

relationship between the medium and the electrolyte electrical conductivities given by

$$\sigma = \sigma_w S_w^n \phi^m \tag{2}$$

where S_w (no units) is the water saturation and ϕ (no units) the porosity of the medium; and exponents n and m (no units) are the so-called saturation and cementation factors, respectively. Several authors have found that these empirical factors depend on the geometry of the pore system or its connectivity (e.g., Knight and Endres, 2005; Glover, 2017; Jougnot et al., 2018). From Archie's pioneer work to the present, numerous theoretical models have been developed within different frameworks such as effective medium, percolation theory or capillary tube models (e.g., Sen et al., 1981; Herrick and Kennedy, 1994; Wang et al., 2007; Cai et al., 2017). Some models account for the surface electrical conduction through porous media which occurs in the vicinity of the solid surface of the pores (e.g. Waxman and Smits, 1968; Bussian, 1983; Thanh et al., 2019, 2020). Based on Archie's law and a volume-averaging approach, Linde et al. (2006) proposed a relationship to estimate the electrical conductivity that accounts the surface conductivity under partially saturated conditions and can be expressed as:

$$\sigma = \phi^m [\sigma_w S_w^n + (\phi^{-m} - 1)\sigma_s]. \tag{3}$$

Several phenomena such as hysteresis effects and reactive processes affect the electrical conductivity (e.g. Binley and Kemna, 2005). Hysteresis refers to the non-unique relationship between electrical conductivity and pressure head or water saturation, which means that different curves can be obtained during sequences of wetting and drying cycles of a porous medium. The variations produced in the electrical conductivity are related to changes in pore fluid distribution caused by changes in the saturation history. The structure of pore space patterns plays a significant role in understanding the flow distribution and predicting the electrical conductivity (Sun et al., 2021). Therefore, an impact at the hysteresis cycle should be observed for porous media under partial saturation as reactive processes produce variations of the pore space geometry. To the best of our knowledge, studies of hysteresis effects during dissolution or precipitation processes are lacking in the literature because they focus more on reactive transport description (e.g. Léger et al., 2022b) rather than water saturation perturbations (e.g. Rembert et al., 2023b). Nevertheless, various works under partially saturated conditions have observed the presence of hysteresis in electrical measurements. Longeron et al. (1989) found that the electrical resistivity of sandstone and limestone samples with a mixture of oil and brine varied with saturation during imbibition and drainage experiments. Knight (1991) observed that hysteresis exists in electrical conductivity data at intermediate water saturations and compared the pore fluid distribution at drainage and imbibition to analyze the phenomenon. Elashahab et al. (1995) studied the effects of hysteresis through saturation history on electrical conductivity for sandstone rocks of different wetting characteristics. Verwer et al. (2011) observed that the two-phase flow electrical resistivity curve exhibits higher values during drainage than imbibition. Mohammadmoradi et al. (2016) developed a pore morphology approach to predict electrical conductivity in porous media during a

hysteresis loop. They remarked that neglecting the hysteresis leads to dramatic errors between the measured and the simulated parameters. Therefore, it is necessary to fully account for the hysteresis behavior for an accurate flow description and electrical conductivity prediction when performing a numerical simulation. Furthermore, a considerably large amount of research studies has been conducted to analyze the different aspects of reactive behaviors of carbonate rocks at total saturation conditions, such as wormholes and their complex relationship with transport properties or changes in the dissolution rate constant (e.g., Alkattan et al., 1998; Liu et al., 2005; Kaufmann and Dreybrodt, 2007; Noiriel et al., 2004; Garing et al., 2015). Among experimental works on the electrical monitoring of dissolution/precipitation processes, Wu et al. (2010) monitored calcite precipitation on a glass beads column and observed the evolution of this process from electrical conductivity data. These results have been confirmed by other studies (e.g., Saneiyan et al., 2019; Izumoto et al., 2020, 2022). Garing et al. (2014) characterized natural carbonate samples presenting high heterogeneity resulting from many dissolution and precipitation processes by measuring the electrical conductivity. However, they did not monitor electrical conductivity changes caused by these reactive processes. Cherubini et al. (2019) analyzed the increase in the electrical conductivity values due to the dissolution of calcite in limestones samples. In the numerical field, Niu and Zhang (2019) simulated the dissolution and precipitation on digital representations of microstructural images to study the electrical conductivity. Even though they observed changes in this electrical property values, no significant variations were estimated in other petrophysical parameters, such as porosity. More recently, Rembert et al. (2023a) studied the impact of conduits formation in limestone samples on the electrical conductivity measurements due to calcite dissolution and the relationship between electrical properties and the evolution of structural parameters over time.

The framework of capillary tube models has been useful to provide valuable insights into different transport phenomena occurring in porous media from the microscopic standpoint (e.g., Celia et al., 2004; Jackson, 2010; Jougnot et al., 2012; Luo et al., 2023; Thanh et al., 2023). In addition, petrophysical properties can be directly calculated in these type of models by simply analyzing the capillary tubes geometry (e.g., Guarracino et al., 2014; Rembert et al., 2020; Soldi et al., 2017, 2022). Because of these advantages, capillary tube models have been extensively used considering different pore size distributions to upscale the petrophysical properties from the contribution of one capillary (e.g., multimodal, quasi-fractal, fractal or gaussian, see Jougnot et al. (2019)). Among them, the fractal distributions have proven to be efficient to represent porous media due to their simplicity and capacity to describe a wide range of natural geological media (e.g. Guarracino, 2006; Yu, 2008; Guarracino and Quintana, 2009; Ghanbarian-Alavijeh et al., 2011). Recently, Soldi et al. (2022) derived an analytical model to estimate the hydraulic properties of porous media under partially saturated conditions. They assumed piecewise sinusoidal variations of the capillary radii along its length which allowed them a more realistic description of the porous media. Indeed, the periodic reductions assumed on the pore structure are defined by two geometrical parameters whose range of values allows the representation of the hydraulic properties for different soil textures.

Electrical properties have been successfully studied within the capillary tube models and fractal distributions. In the last years, Thanh et al. (2019, 2020) derived electrical conductivity models for total and partially saturated porous media accounting for surface conductivity. For both models, they assumed that the bundle of capillaries follows a fractal pore size distribution and that each capillary is represented by a tortuous cylindrical tube of constant radius. Chen et al. (2023) derived a theoretical correlation between the formation factor and tortuous pore structure with a wide distribution of pore sizes. The authors also consider cylindrical tubes of constant radii, however, they propose that tortuosity follows a fractal law. Saafan et al. (2023) developed a model to describe the electrical conductivity for a reservoir porous medium where the fluid phases are water and oil. They represented the partially saturated pore system using tortuous fractal capillaries with constant square or triangular cross-sectional areas. Nevertheless, these models are lacking an important microstructure parameter which significantly controls the transport and petrophysical properties of porous media, the constrictivity. This parameter characterizes the so-called bottleneck effect that means that the wide spaces of the pores or pore bodies are connected through pore throats (i.e. non-constrictive and constrictive lengths). The previously described models do not account for this type of variations in the capillary radii along their length which should be considered to provide a more accurate description of porous media in the framework of capillary bundles. In this work, we derive an analytical model that considers a realistic pore geometry to estimate the electrical conductivity under partially saturated conditions. Based on the framework of capillary tube models and the geometry proposed by Soldi et al. (2022), the pore space is represented by a bundle of cylindrical capillaries with varying aperture along their pore length to take into account the structure composed of pore throats and pore bodies. This geometry has the advantage to represent a wide range of pore geometries due to the variable lengths of the pore throats and pore bodies. The proposed model is an extension of the model developed by Rembert et al. (2020) that estimates the electrical conductivity for total saturated porous media. Their model considers the pores as tortuous cylindrical tubes with sinusoidal variations of their aperture. Assuming a fractal pore size distribution that can be either filled by water or by air, we obtain mathematical closed-form expressions to estimate the saturated and relative electrical conductivity from the upscaling procedure. The macroscopic expression relies on geometrical parameters defining the pore structure (e.g., the constrictivity), tortuosity, pore-size distribution, and radii of the pores. The pore throats and pore bodies present in the proposed geometry allow us to include the hysteresis phenomenon in the relative electrical conductivity. Considering the structural variations that reactive processes can cause, we describe the temporal evolution of the saturated electrical conductivity by assuming a constant dissolution of the pores. The performance of the model to reproduce experimental data is tested against different sets of laboratory data of soils with varied textures.

2 Electrical conductivity model

The present model is derived based on the pore geometry proposed by Soldi et al. (2022) and follows the work developed by Rembert et al. (2020). Within the framework of capillary tube models, we consider a porous medium represented by an ensemble of tortuous constrictive capillaries in a cylindrical representative elementary volume (REV) of radius R_{REV} (m) and length L (m). Since we focus on the porous microstructure, we consider that the surface conductivity is negligible. However, similar developments could be done including the surface conductivity (e.g. Thanh et al., 2020; Luo et al., 2023).

2.1 Pore space description

At the microscopic scale, we consider that each pore of the capillary bundle is represented by a tortuous cylindrical tube with varying aperture (see Fig. 1). All the pores are assumed to have the same length l (m) and tortuosity τ ($\tau = l/L$, no units). The pore radius varies along all the length of each capillary between its radius value R (m) and its pore throat radius value aR (m) where a (no units) is the radial factor that quantifies the reduction in the pore radius due to the presence of the constrictivity. A sinusoidal piecewise geometry is assumed with a wavelength λ (m) which replicates along the pore length (i.e. $l \gg \lambda$). Thus, the varying radius $r(x)$ (m) of a capillary can be expressed as (Soldi et al., 2022):

$$r(x) = \begin{cases} (1+a)\frac{R}{2} + (1-a)\frac{R}{2}\sin\left(\frac{\pi x}{\lambda(1-c)}\right) & \text{if} \quad x \in [0, \lambda(1-c)) \\ (1+a)\frac{R}{2} + (1-a)\frac{R}{2}\sin\left(\frac{\pi[x-\lambda(1-2c)]}{\lambda c}\right) & \text{if} \quad x \in [\lambda(1-c), \lambda), \end{cases} \tag{4}$$

where c (no units) is the length factor which represents the constrictive fraction of λ (i.e. the segment of λ where the radius is reduced). The geometrical factors a and c vary between 0 and 1. Note that the limit values $a = 0$ and $a = 1$ correspond to the cases of periodically closed pores and cylindrical pores of constant radius R, respectively. Also note that if $c = 0.5$, the proposed geometry is consistent with the geometry proposed by Guarracino et al. (2014) and Rembert et al. (2020) that considers equal lengths for the constrictive and non-constrictive fractions of the wavelength.

The porous structure of the medium is assumed to be a bundle of capillary tubes with different sizes of radii varying from a minimum pore radius R_{min} to a maximum pore radius R_{max}. Based on the fractal theory for porous media (e.g. Tyler and Wheatcraft, 1990; Yu et al., 2003; Liang et al., 2014), the pore size distribution can be described by the following fractal law:

$$N(R) = \left(\frac{R_{REV}}{R}\right)^D, \tag{5}$$

where $N(R)$ (no units) is the number of pores whose radii are greater than or equal to R and D (no units) is the pore size fractal dimension. Considering the classical fractal object called Sierpinski carpet, Tyler and Wheatcraft (1990) show that this parameter D

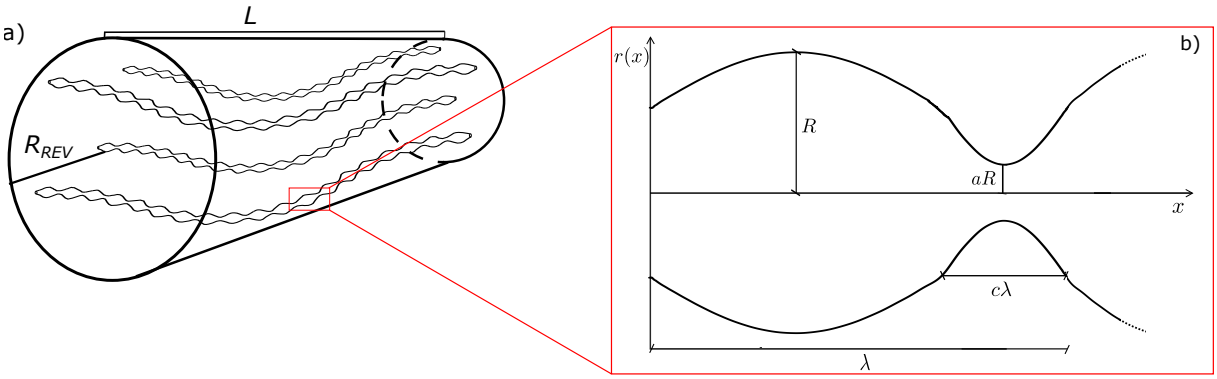

Figure 1: (a) Sketch of the representative elementary volume represented by a bundle of tortuous sinusoidal capillary tubes, and (b) the pore geometry considered for each piecewise sinusoidal capillary.

varies between 1 and 2 for different textures of porous media where its highest values are associated with the finest textured soils.

Then, the number of pores whose radii are within the infinitesimal range R and $R+dR$ is obtained from Eq. (5) by differentiating with respect to R:

$$-dN(R) = DR_{REV}^{D} R^{-D-1} dR, \tag{6}$$

where the minus sign implies that the pore number increases when the pore radius decreases (e.g. Yu et al., 2003; Yu, 2008).

2.2 Electrical conductivity model

2.2.1 Electrical model at saturation

To derive the expressions of the new electrical conductivity model, we first describe the electrical properties of a single capillary. For a water saturated capillary of radius R, its electrical conductance $\Sigma_p(R)$ (S) can be calculated as:

$$\Sigma_p(R) = \int_0^l \frac{1}{\sigma_w \pi r^2(x)} dx. \tag{7}$$

By replacing Eq. (4) in Eq. (7) yields:

$$\Sigma_p(R) = \frac{\sigma_w \pi R^2 f(a,c)}{\tau L}, \tag{8}$$

$$f(a,c) = \frac{2a^{3/2}}{1+a}\left\{1 + (2c-1)\left[\frac{4\sqrt{a}(1-a)}{\pi(1+a)^2} + \frac{2}{\pi}\tan^{-1}\left(\frac{1-a}{2\sqrt{a}}\right)\right]\right\}^{-1}. \tag{9}$$

The factor $f(a,c)$ (no units) varies between 0 and 1, and quantifies the reduction in the conductance of each pore due to the presence of the pore throats (i.e. the so-called constrictivity).

The contribution of each single capillary conductivity $\sigma_p(R)$ (S m^{-1}) to the porous medium conductivity is then obtained by multiplying the pore conductance (Eq. (8)) with a geometric factor $f_g = \pi R_{REV}^2/L$ (m) (Hem and Minear, 2012; Rembert et al., 2020):

$$\sigma_p(R) = \frac{\sigma_w R^2 f(a,c)}{\tau R_{REV}^2}. \tag{10}$$

According to Ohm's law, the electric current $i_p(R)$ (A) flowing between the edges of a capillary of radius R is directly proportional to the electrical voltage difference ΔV (V) across them:

$$i_p(R) = \Sigma_p(R)\Delta V = \frac{\sigma_w \pi R^2 f(a,c)}{\tau L}\Delta V. \tag{11}$$

For a fully saturated porous medium, the total electric current I^{REV} (A) flowing through the REV is obtained from Kirchhoff's current law, by summing the electric currents contributions of all the capillaries over the entire range of pore sizes:

$$I^{REV} = \int_{R_{min}}^{R_{max}} i_p(R) dN(R). \tag{12}$$

Substituting Eqs. (6) and (11) in Eq. (12) and integrating it yields to

$$I^{REV} = -\frac{\sigma_w \pi R_{REV}^D D f(a,c)}{\tau L(2-D)} \left(R_{max}^{2-D} - R_{min}^{2-D}\right) \Delta V. \tag{13}$$

On the other hand, based on Ohm's law at the REV scale, the total electric current I^{REV} flowing through the porous medium can be expressed as:

$$I^{REV} = -\sigma^{REV} \pi R_{REV}^2 \frac{\Delta V}{L}, \tag{14}$$

where σ^{REV} (S m^{-1}) is the electrical conductivity of the porous medium which under total saturated conditions is redefined as the saturated electrical conductivity σ_{sat}^{REV}. Combining Eqs. (13) and (14), an expression for σ_{sat}^{REV} is obtained:

$$\sigma_{sat}^{REV} = \frac{\sigma_w D f(a,c)}{\tau R_{REV}^{2-D}(2-D)} \left(R_{max}^{2-D} - R_{min}^{2-D}\right). \tag{15}$$

The capability to estimate the electrical conductivity σ_{sat}^{REV} of a porous medium as a function of the medium's porosity ϕ is significantly valuable in petrophysics. For the proposed model, a relationship between these two macroscopic properties can be obtained by considering that for this porous medium geometry its porosity ϕ is given by (Soldi et al., 2022):

$$\phi = \frac{D\tau f_v(a,c)}{R_{REV}^{2-D}(2-D)} \left(R_{max}^{2-D} - R_{min}^{2-D}\right) \tag{16}$$

where $f_v(a,c) = (1+a)^2/4 + (1-a)^2/8 + (1-a^2)(1-2c)/\pi$ is a factor that quantifies the reduction in the porosity of the REV due to the presence of the constrictivities (the subscript v stands for volume). Then, combining Eqs. (15) and (16) yields:

$$\sigma_{sat}^{REV} = \frac{\sigma_w f_\sigma(a,c)\phi}{\tau^2} \tag{17}$$

where f_σ is a dimensionless factor that varies between 0 and 1, and is defined as the ratio between the factor f and f_v. The exact expression of f given in Eq. (9) can be reduced similar to Soldi et al. (2022) and f_σ can be expressed as:

$$f_\sigma(a,c) = \frac{16\pi^2 a^{3/2}(1+a)}{[\pi(1+a)^2 + 2(2c-1)(1-a)(1+\sqrt{a})^2][2\pi(1+a)^2 + \pi(1-a)^2 + 8(1-a^2)(1-2c)]}. \tag{18}$$

The variation of the factor f_σ as a function of the radial factor a is shown in Fig. 2, for different values of the length factor c. Note that the presence of the pore throats affects significantly the electrical conductivity of the REV σ_{sat}^{REV} through the f_σ values which depends on a. Also note that if $a = 0$, $f_\sigma = 0$ and $\sigma_{sat}^{REV} = 0$, no electrical conduction takes place in the REV as the pores are periodically closed. In that case, $f_v \neq 0$ which means that the REV has a porosity value but the pores are not connected. In order to represent this type of porous media using Archie (1942), $\sigma = 0$ only in the case that $\phi = 0$. Therefore, Archie (1942) cannot represent this media, while the proposed model can describe media with a porosity that corresponds to poorly connected pores, and low electrical conductivity. The expression of the factor f_σ given by Eq. (18) can be reduced while taking into account the main features of the factor's behavior and it yields

$$g_\sigma(a,c) = \frac{8a^{3/2}}{(1+a)\left[(1+a)^2 - (1-a)^2(1-6c+6c^2)\right]}. \tag{19}$$

This simplified expression is easier to evaluate and, therefore, its implementation in numerical codes is straightforward.

Eqs. (15) and (17) are closed-form expressions that describe the saturated electrical conductivity σ_{sat}^{REV} of the medium which depend on the water electrical conductivity, porosity and model parameters with physical or geometrical meaning. It is interesting to observe that the estimates of σ_{sat}^{REV} are strongly influenced by the parameters a and c of the pore geometry through the factor f_σ. In the limit case of $a = 1$ and $\tau = 1$, Eq. (17) becomes $\sigma_{sat}^{REV} = \sigma_w\phi$ which is consistent with Archie's law expression for $m = 1$ where the porous medium is composed by a bundle of non-tortuous capillaries of constant radii (e.g., Clennell, 1997). For tortuous capillary bundles, the relationship between tortuosity and porosity can be expressed by the Bruggeman relation, i.e., $\tau^2 = \phi^{-1/2}$ (Holzer et al., 2023). Substituting this relation in Eq. (17), we obtain a porosity with an exponent equal to 1.5 which is consistent with the m value observed by Sen et al. (1981) for ideally packed spheres. Note also that, if $c = 0.5$, the resulting expressions of Eqs. (15) and (17) are similar to the ones proposed by the model of Rembert et al. (2020).

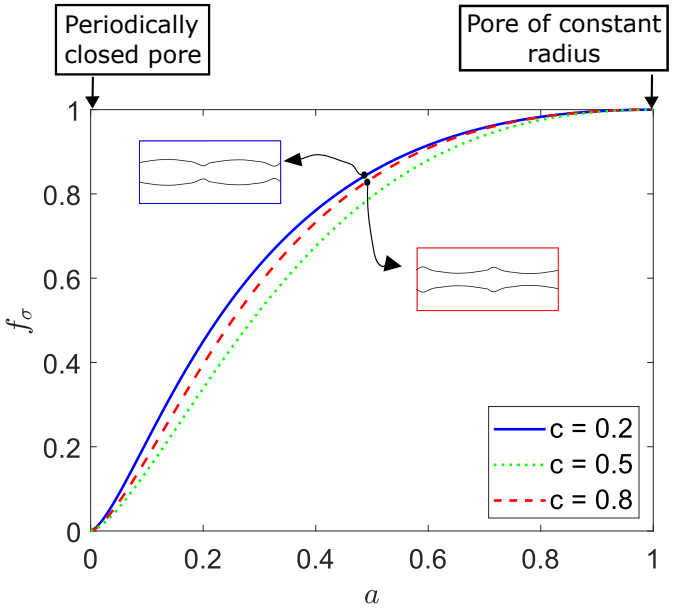

Figure 2: Dimensionless constrictivity factor f_σ (Eq. (18)) as a function of the radial factor a for different constant values of the length factor c.

2.2.2 Effect of partial saturation and hysteresis

Under the hypothesis of neglecting surface conduction, the electrical conductivity of the REV under partially saturated conditions can be expressed as

$$\sigma^{REV} = \sigma_{sat}^{REV} \sigma_{rel} \tag{20}$$

being σ_{rel} (no units) the relative electrical conductivity of the REV. To obtain the expression of σ_{rel}, we consider a similar derivation procedure as for the total saturated porous medium but with capillaries that can be either fully saturated by water or by air (e.g., Soldi et al., 2017; Thanh et al., 2020). Following the procedure proposed by Guarracino et al. (2014), we assume that the REV is fully saturated at its initial state and then is drained when subjected to a pressure head h (m). To determine which pores will be desaturated by the applied pressure head, h, under a Darcy's flow regime (i.e., low Reynolds number), we consider the link between the radius of the water-filled pore R_h (m) to the pressure head h given by (e.g. Jurin, 1717)

$$h = \frac{2T_s \cos(\gamma)}{\rho_w g R_h}, \tag{21}$$

where T_s (N m^{-1}) is the surface tension of the water, γ (°) the contact angle, ρ_w (kg m^{-3}) the water density and g (m s^{-2}) the gravitational acceleration. A capillary tube becomes fully desaturated if the radius of its pore throat aR is greater than the radius R_h defined by Eq. (21). Thus, for the drainage process, it is reasonable to assume that pores with radii R between R_{min} and R_h/a will remain fully saturated and contribute to the electric

current flowing through the REV. If we now consider an imbibition process where the REV is dry at the beginning and flooded by a pressure head h, the capillary tubes that will be fully saturated in this case are those whose radii R are smaller than R_h. Then, considering the ranges of saturated pores for each process, the electrical current streaming through the REV (Eq. (12)) can be expressed as:

$$I^{REV} = \int_{R_{min}}^{R^*} i_p(R) dN(R) \tag{22}$$

where $R^* = R_h/a$ for the drainage and $R^* = R_h$ for the imbibition. Combining Ohm's law at macroscale (Eq. (14)) with Eq. (20), and comparing it with the result of integrating Eq. (22), we obtain the expression for the relative electrical conductivity σ_{rel}:

$$\sigma_{rel}(R^*) = \frac{R^{*2-D} - R_{min}^{2-D}}{R_{max}^{2-D} - R_{min}^{2-D}}. \tag{23}$$

Substituting Eq. (21) in (23), the relative electrical conductivity can be expressed as function of the pressure head for a drainage process as:

$$\sigma_{rel}^{d}(h) = \frac{(ah)^{D-2} - h_{max}^{D-2}}{h_{min}^{D-2} - h_{max}^{D-2}} \tag{24}$$

where h varies between $\frac{h_{min}}{a}$ and $\frac{h_{max}}{a}$, and for an imbibition process, it yields:

$$\sigma_{rel}^{w}(h) = \frac{h^{D-2} - h_{max}^{D-2}}{h_{min}^{D-2} - h_{max}^{D-2}} \tag{25}$$

where h varies between h_{min} and h_{max}. By inspection of Eq. (24), note that if $h < \frac{h_{min}}{a}$, $\sigma_{rel}^{d} = 1$, since the REV is fully saturated as the pressure head applied is lower than the one necessary to start draining the larger pores, and in the case of $h > \frac{h_{max}}{a}$, $\sigma_{rel}^{d} = 0$ as the pressure head applied is large enough to drain the REV. Similar results can be obtained by analyzing Eq. (25) for the imbibition process, $\sigma_{rel}^{d} = 1$ and $\sigma_{rel}^{d} = 0$, when $h < h_{min}$ and $h > h_{max}$, respectively. Note that the σ_{rel} expression differs between the drainage and imbibition processes due to the presence of the pore radius reduction defined by the radial factor a. Therefore, these irregularities present in the pore geometry allow to introduce the hysteresis phenomenon in the electrical conductivity model. This fact has also been remarked by Singha et al. (2007), who explain solute transport hysteresis effects in the electrical conductivity though a bicontinuum model composed by mobile (i.e., well-connected) and immobile (i.e., poorly-connected) pores. Fig. 3 shows the hysteresis cycle on this electrical property for different values of the radial factor a. For the remaining parameters of Eqs. (24) and (25), we considered the following constant values: $D = 1.5$, $h_{min} = 0.01$ m and $h_{max} = 10$ m. It can be seen that the radial factor a significantly affects the main drying curves of the relative electrical conductivity while no variations are produced on the main wetting curves of this electrical property since they are independent of a. Indeed, low values of a produce a shift of the main drying σ_{rel} curves to higher values

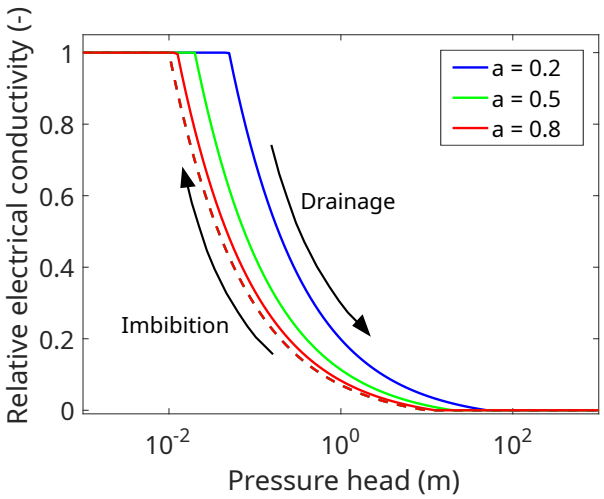

Figure 3: Hysteresis cycle of the relative electrical conductivity as function of pressure head for different values of the radial factor a. The solid and dashed lines correspond to the main relative electrical conductivity curves for drainage and imbibition experiments (Eqs. (24) and (25)), respectively. Note that all the imbibition curves are superimposed.

of the pressure head as higher pressure head values are needed to drain more constrictive pores. Also note that, in the limit case of a approaching 1, the two σ_{rel} curves tend to reduce their distance, as it can be expected since this situation represents capillary tubes of constant radii and thus no hysteretic phenomenon will be observed.

For partially saturated conditions, the behaviour of the relative electrical conductivity is often described by its dependence with the water saturation S_w (no units). Within the framework of capillary tube models, the effective saturation S_e (no units) is the variable most used since the tubes are fully saturated or empty, and is related to S_w through

$$S_w = (1 - S_r)S_e + S_r \tag{26}$$

where S_r (no units) is the residual water saturation. Recently, Soldi et al. (2022) developed an analytical model for the hydraulic properties of a porous medium with the geometry considered for the proposed electrical model. Note that saturation is obtained from an equation which is identical to Eq. (23). Therefore, for the proposed model the relationship between σ_{rel} and S_e yields:

$$\sigma_{rel}(S_e) = S_e. \tag{27}$$

From a theoretical point of view, it can be observed that Eq. (27) results in a non-hysteretic function, while Eqs. (24) and (25) account for the hysteresis phenomenon.

2.2.3 Evolution of the model in reactive media

The electrical conductivity can be affected by dissolution and precipitation processes particularly in porous media composed by carbonate minerals. When a fluid flows through a

reactive porous medium produces changes in the structure of the pore space causing variations of its volume and surface. In order to estimate the resulting geometrical changes, we assume that each capillary tube is dissolved uniformly so that its circular cross-sectional shape is retained while only increasing its radius. Then, to evaluate how dissolution affects the pore structure, we assume that the volume change of a pore with time t is proportional to the pore surface S_p that is in contact with the reactive fluid and to the dissolution rate α (Freedman et al., 2004; Guarracino et al., 2014):

$$\frac{dV_p(R)}{dt} = S_p(R)\alpha(R). \tag{28}$$

Whereas dissolution will only occur in water-saturated pores, for further developments and similar to the film depositional model proposed by Freedman et al. (2004), we assume that this reactive process affects all pore radii. Note that in Eq. (28), the dissolution rate depends on the pore radius value ($\alpha(R)$) since large pores enlarge faster than small pores during dissolution (e.g. Schechter and Gidley, 1969). We assume a linear dependence between these variables (i.e. $\alpha(R) = \tilde{\alpha}R$) since a constant rate would reflect an extremely slow dissolution independent of the actual occuring dissolution along the flow path. In the other extreme, a relationship with a higher exponent would reflect a very aggressive dissolution which could lead to wormholes (e.g., Noiriel et al., 2004). Under this linear rate hypothesis, the fractal dimension and the radial and length factors can be assumed constant during the reactive process. Integrating Eq. (28), we obtain the evolution with time of a pore radius (Guarracino et al., 2014):

$$R(t) = R(t_0)e^{\beta(t-t_0)} \tag{29}$$

being t_0 (h) the initial time of the dissolution process and factor β (h^{-1}) a function of the model parameters a, c and $\tilde{\alpha}$ (h^{-1}) given by (Soldi et al., 2024):

$$\beta = \frac{\tilde{\alpha}[4\pi(1+a)c + (1-a)(1-2c)]}{2\pi(1+a)^2 + \pi(1-a)^2 + 8(1-a^2)(1-2c)}. \tag{30}$$

Note that for a dissolution process both $\tilde{\alpha}$ and β are positive parameters. Under the same hypotheses and considering that parameter $\tilde{\alpha} < 0$, we can derive a similar expression to Eq. (29) where $\beta < 0$ (i.e. a decreasing radius with time) which allows us to describe the reduction of the pore volume with time that occurs during a precipitation process.

The evolution of the electrical conductivity during reactive processes can be obtained by considering the changes of the pore radii R_{min} and R_{max} with time. Substituting Eq. (29) in Eq. (15), the temporal variation of this macroscopic property for saturated conditions can be expressed as:

$$\sigma_{sat}^{REV}(t) = \sigma_{sat}^{REV}(t_0)e^{\beta(2-D)(t-t_0)} \tag{31}$$

where $\sigma_{sat}^{REV}(t_0)$ is the electrical conductivity of the REV at the initial time t_0 of the dissolution process. For partially saturated conditions, at each time of a dissolution

process, the pressure head needed to drain or flood the REV is related to the size of the pore throat and pore body radii for the drainage and imbibition processes, respectively. Therefore, the relative electrical conductivity (Eqs. (24) and (25)) depends on time and for a drainage process it can be expressed as

$$\sigma_{rel}^{d}(h,t) = \frac{(ah)^{D-2}e^{\beta(D-2)(t-t_0)} - h_{max}^{D-2}(t_0)}{h_{min}^{D-2}(t_0) - h_{max}^{D-2}(t_0)} \tag{32}$$

where h varies between $h_{min}(t_0)e^{-\beta(t-t_0)}/a$ and $h_{max}(t_0)e^{-\beta(t-t_0)}/a$. While for an imbibition process, the relative electrical conductivity yields

$$\sigma_{rel}^{w}(h,t) = \frac{h^{D-2}e^{\beta(D-2)(t-t_0)} - h_{max}^{D-2}(t_0)}{h_{min}^{D-2}(t_0) - h_{max}^{D-2}(t_0)} \tag{33}$$

where h varies between $h_{min}(t_0)e^{-\beta(t-t_0)}$ and $h_{max}(t_0)e^{-\beta(t-t_0)}$. The terms $h_{min}(t_0)$ and $h_{max}(t_0)$ are the minimum and maximum pressure heads at the beginning of the dissolution process. Given the exponential nature of Eqs. (29), (31), (32), and (33), we perform a parametric analysis of the exponent parameter β (Eq. (30)). Fig. 4 shows the role of the model's geometric parameters (a and c) in the estimates of parameter β for a constant dissolution rate of $\tilde{\alpha} = 0.0001\ h^{-1}$. Note that for a high value of c and low values of a (i.e., a long pore-throat length and important pore radius reduction), the values of parameter β increase significantly as dissolution will produce a significant opening of the pore. Therefore, as the flow increases through the capillaries, so does the electrical conductivity. It can also be observed that for high values of parameter a and low values of c (i.e., capillaries with a slight pore throat), parameter β has the lowest value. This means that the radius of the pores will increase with the dissolution without significant changes occurring in the constrictive geometry as the capillary is almost a cylindrical tube. From Eq. (30) it can be seen that the value of β remains constrained in the range $0 \leq \beta \leq \frac{4\pi-1}{3\pi-8}\tilde{\alpha} \approx 8.12\tilde{\alpha}$. Indeed, as the magnitude of the dissolution rates $\tilde{\alpha}$ are very low, parameter β cannot take a significant value. Note also that when the radii of the pores increase, the pressure head needed to drain or flood the *REV* decreases, and the hysteresis cycle of the final stage of dissolution is shifted to the left of the cycle from the beginning of the process.

The model proposed in this section is developed within the framework of capillary tube models. One of the limitations that affect the models based on this framework is that lateral connection between the capillaries is not considered. There are no intersection points among the pores and they all have parallel directions. However, many models of electrical properties have been developed in this framework and successfully proven to provide good estimates of electrical and hydraulic properties (e.g., see comparison between 2D pore networks and capillary bundle models in Jougnot et al., 2019). A second point of concern in the model regards the relatively high number of model parameters compared to previous models such as the empirical model of Archie (1942) which has only two parameters (cementation and saturation exponents). Nevertheless, the proposed theoretical model can be used for any porous media while Archie (1942) cannot represent

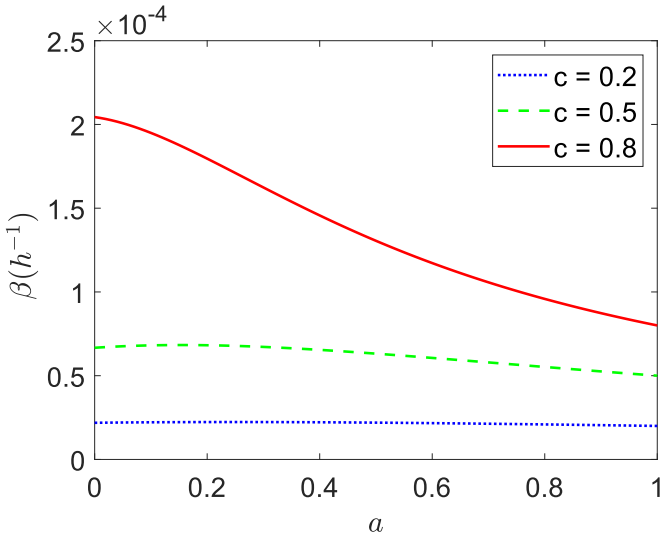

Figure 4: Parametric analysis of the factor β as a function of the radial factor a for different constant values of the length factor c and a constant value of the dissolution rate $\tilde{\alpha} = 0.0001\ h^{-1}$.

media with high porosity and low electrical conductivity. Beyond that, a step forward of the proposed model over the classical is that it accounts for phenomena such as the hysteresis effects or dissolution/precipitation. One last point of the proposed petrophysical model is that these reactive processes are considered through their effect on the pore geometry changes, while chemical variations, such as changes on salinity or pH, are neglected. These variations were taken into account in the geochemical model proposed by Rembert et al. (2022), and in the works of Leroy et al. (2017) and Heberling et al. (2021) who developed geochemical models that consider surface alterations. Note that, while other electrical models can be used to estimate the electrical conductivity, the proposed model can explicitly relate parameters linked to the microstructure to the estimates of the property at the macroscale, and with only one set of them is also capable to account for hysteresis effects and reactive processes.

3 Model comparison with experimental data

The proposed model ability to estimate the electrical conductivity is tested against different sets of experimental data from the research literature. These data sets consist of measured electrical conductivity or relative electrical conductivity values for different soil textures.

3.1 Electrical conductivity data for different soil textures

In order to test the estimates of the proposed model, we selected experimental data sets from different soil textures: a sandy loam from Amente et al. (2000), a sand from Inoue et al. (2000), a loam from Doussan and Ruy (2009) and a packing of mica particles from Friedman and Robinson (2002). These data series consist of electrical conductivity or relative electrical conductivity values as a function of saturation. As mentioned is Section 2, the proposed model assumes that the surface electrical conduction is negligible and the electrical conductivity is due to the conduction in the porous water. However, the values of surface conductivity for soils can impact the experimentally measured values of soil conductivity. We account for the contribution of the surface conductivity σ_s as a parallel conductivity with an adjustable value, therefore, considering Eqs. (15), (27) and (26), the model expression as function of water saturation becomes:

$$\sigma^{REV}(S_w) = \frac{\sigma_w f_\sigma(a,c)\phi}{\tau^2(1-S_r)}(S_w - S_r) + \sigma_s. \tag{34}$$

Equation (34) is also compared with the Waxman and Smits (1968) model:

$$\sigma_{WS}(S_w) = \frac{S_w^n}{F}\left(\sigma_w + \frac{\sigma_s^{WS}}{S_w}\right) \tag{35}$$

where the formation factor F is related to porosity ϕ through $F = \phi^{-m}$. The relative electrical conductivity values $\sigma_{rel}^{REV}(S_w)$ can be estimated, for both models, as the quotient between the electrical conductivity value as function of saturation $\sigma^{REV}(S_w)$ and its value at total saturation $\sigma^{REV}(S_w = 1)$. The proposed model is fitted by an exhaustive search method by minimizing the normalized mean square error ($NMSE$) between the calculated and the experimentally measured values. The comparison between the proposed model and the different experimental data is shown in Figure 5 and the model of Waxman and Smits is also shown. Tables 1 and 2 list the best fitted parameters of the proposed model (a, c, τ, S_r and σ_s) and Waxman and Smits model (n, m and σ_s^{WS}), respectively. The values of ϕ and σ_w required by the models are listed in Table 1. By comparing the values of parameter σ_s and σ_s^{WS}, it can be observed that the differences between them is lower for the most conductive electrolytes (i.e., high σ_w) since in those cases the electrical conduction is more significant in the liquid phase than the electrical conduction occurring in the liquid–solid interface. Waxman and Smits (1968) accounted the surface electrical conduction by assuming that this contribution depends inversely with water saturation (Eq. (35)). Therefore, the electrical conduction takes place near the mineral surface for low saturations, while for high saturations the electrical conduction through the electrolyte is the most important contribution. However, the surface conductivity is also dependent on the salinity, the mobility of the ions, and the surface charge density of the EDL (Revil, 2013a). In the proposed model (Eq. (34)), σ_s is treated as a constant for simplicity, not varying with water saturation as assumed by previous works (e.g., Mualem and Friedman, 1991; Friedman, 2005; Laloy et al., 2011; Breede et al., 2011). Even though the differences in the developments of the models, note that the proposed model is able

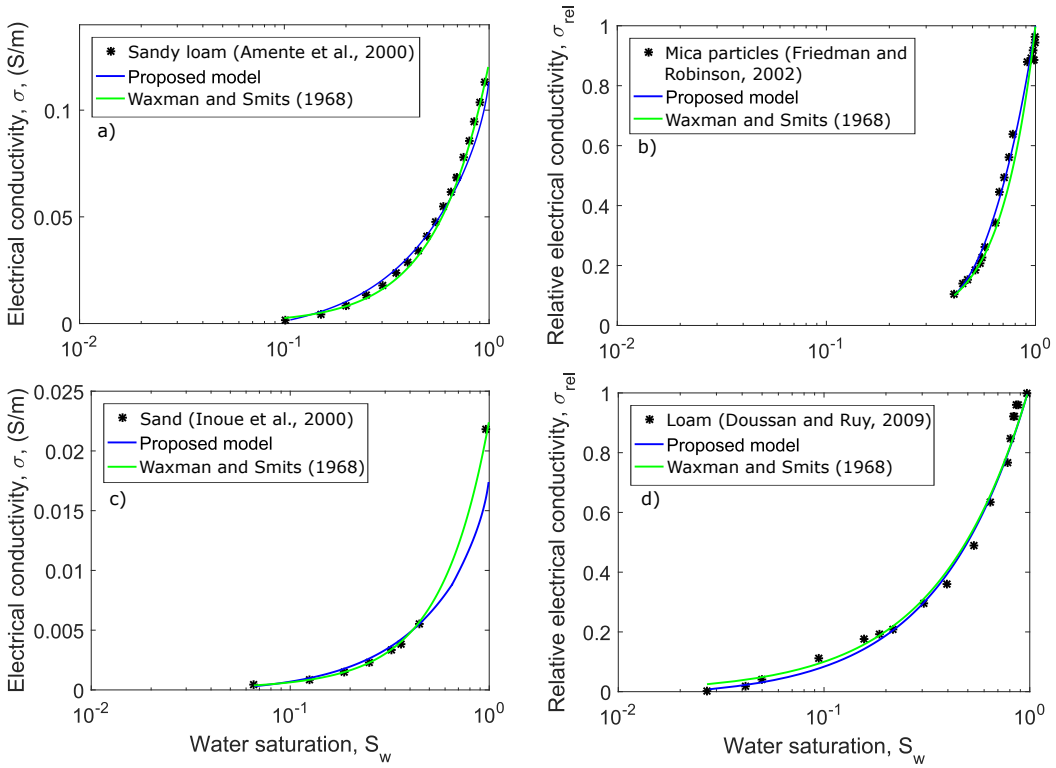

Figure 5: Electrical conductivity as function of water saturation for different data sets: a) a sandy loam from Amente et al. (2000), b) a packing of mica particles from Friedman and Robinson (2002), c) a sand from Inoue et al. (2000) and d) a loam from Doussan and Ruy (2009).

to fairly reproduce the behaviour of the data for the different soil textures and is in good agreement with the previous model of Waxman and Smits.

The experimental samples from Weerts et al. (1999) correspond to four undisturbed soil cores of a loamy sand (named PS9, PS10, PS11 and PS13) where the electrical conductivity was measured as function of water saturation. Figure 6 illustrates the fit of the proposed model (Eqs. (17) and (27)) for the four samples and the best-fitted parameters are listed in Table 3 which were found using the same method as for the previous experimental data sets. It can be observed that the proposed model produces a fairly good agreement with the data sets for all the samples. From the comparison of the fitted model parameter values, note that even though their values differ between the different samples, they vary between close values which can be expected as the samples are from a same soil type. The pore geometry described by these parameters presents smooth changes between the throat and wide pore body. Indeed, the high values of c and a represent that the pore radius varies moderately. We can compare our model performance to the previously published model of Thanh et al. (2020) to fit these experimental data. They derived a model based on a capillary bundle of constant radii pores and proposed a similar number of fitting parameters. Note that our new model performs better than the

one from Thanh et al. (2020), which shows nearly 15% error when it is around 2-3% for our model.

The data from Tartrat et al. (2019) consist on electrical conductivity-water saturation values measured in five core samples. These samples were made of mixes of a background illitic clay material and pyrite grains. The electrical measurements were performed on each sample during their desiccation. This process causes a variation on the water electrical conductivity that cannot be neglected as salinity increases during the decrease of the saturation due to evaporation. To account this phenomenon on the estimates of the electrical conductivity model (Eq. (34)), we assume that the water electrical conductivity increases inversely with saturation during the desiccation process, $\sigma_w(S_w) = \sigma_w(S_w = 1)/S_w$ where the water electrical conductivity at saturation is $\sigma_w(S_w = 1) = 0.115$ S m^{-1} (Tartrat et al., 2019). The performance of the proposed model for the different samples is shown in Figure 7 and Table 4 lists the best fitted parameter values. The porosity value needed to estimate σ_{sat}^{REV} was taken from Tartrat et al. (2019) being its value $\phi = 0.65$. The proposed model is able to fairly well reproduce the behaviour of all the experimental data sets. The values obtained for the geometrical parameters a and c that define the constrictivities of the pores vary between the different samples. However, they remain in a narrow range of values, from 0.40 to 0.63 for a, and from 0.36 to 0.49 for c. These ranges of a and c values represent pores with a fairly significant constrictivity (i.e. a large fraction of the pore with reduced radius) which can be expected since clays present these reductions in the pore structure due to the packing of its fined grains.

Saafan et al. (2023) measured electrical conductivity variations with water saturation in low-permeability sandstone samples, called S6, S9, S13, S14, S16 and S18. The test of the proposed model relies on fitting the electrical conductivity data sets with Eq. (34). As sandstones usually present very low surface conductivities, we considered negligible its contribution to the electrical conductivity. Using an exhaustive search method as previously, we found the best-fitted parameters which are listed in Table 5. To fit these parameters we considered the value of the water electrical conductivity $\sigma_w = 5.38$ S m^{-1} which was taken from Saafan et al. (2023). Figure 8 shows predicted and measured data where it can be observed that the proposed model produces a fairly good agreement for all the samples. The low values of parameter a and high values of c fitted for the proposed model represent pore geometries with a strong reduction of the pore radii along a significant length of the capillary. This pore geometry can be expected since the enclosure of the pore radii hinders the water flow which translates in low permeability samples.

3.2 Electrical conductivity during dissolution

The performance of the model to describe the dissolution phenomenon on the electrical conductivity is tested with experimental data obtained by Rembert et al. (2023a). They measured the evolution of the electrical conductivity σ_{sat}^{REV} with time on two limestone samples, named E04 and E05, during dissolution. Moreover, they also measured the variations of porosity ϕ and permeability k of the sample due to this process. Based on the expressions of ϕ and k developed by Soldi et al. (2022) and considering the changes

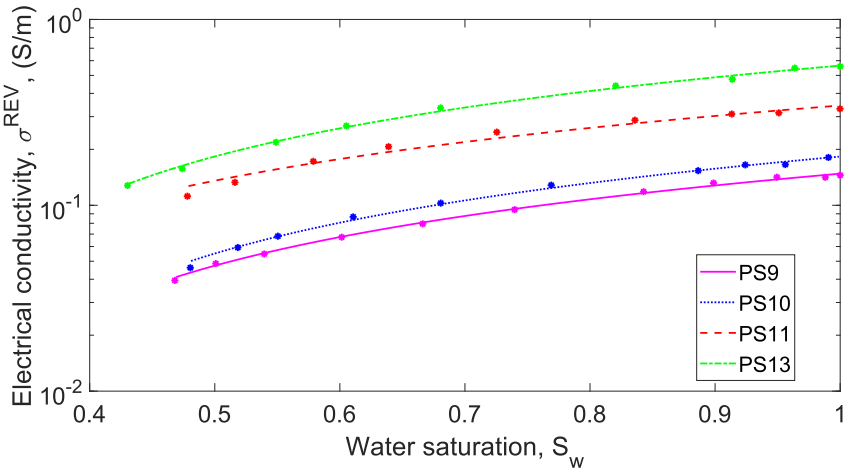

Figure 6: Comparison between the electrical conductivity proposed model (solid lines) and experimental data sets (points) from a loamy sand (Weerts et al., 1999).

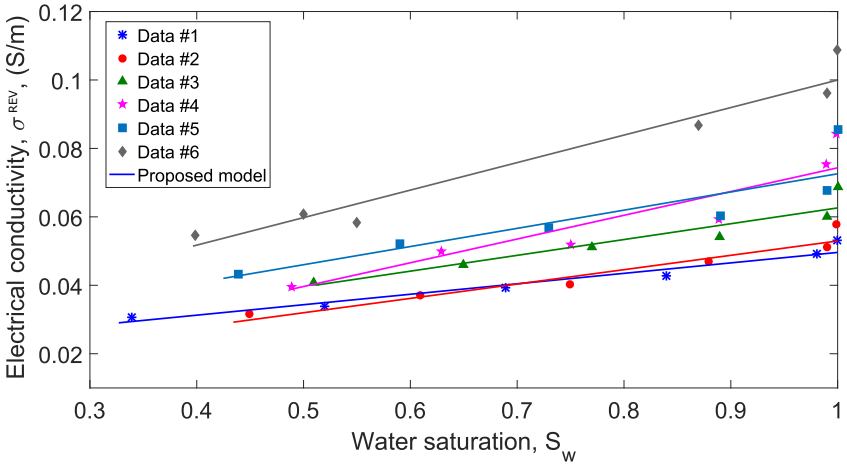

Figure 7: Comparison between the electrical conductivity proposed model (solid lines) and experimental data sets (points) measured in a illitic clay material with pyrite grains from Tartrat et al. (2019).

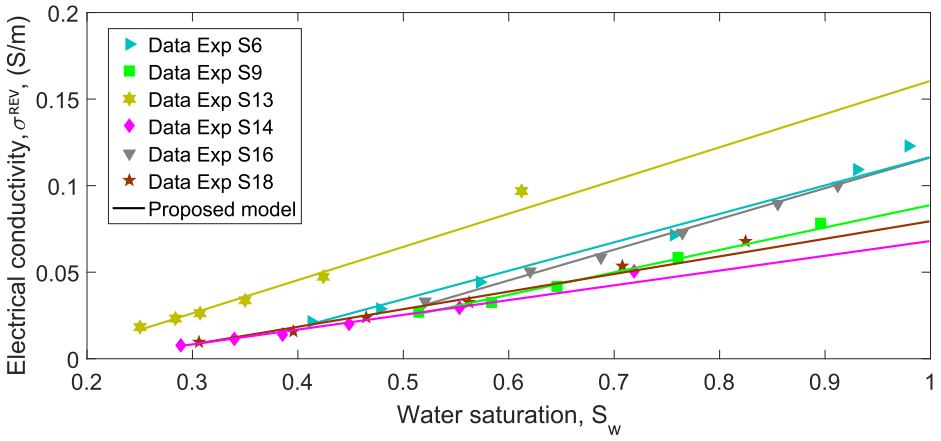

Figure 8: Comparison between the electrical conductivity proposed model (solid lines) and experimental data sets (points) from a low-permeability sandstone from Saafan et al. (2023).

Table 1: Values of the parameters used to estimate the electrical conductivity for experimental data from Amente et al. (2000), Inoue et al. (2000), Friedman and Robinson (2002) and Doussan and Ruy (2009). The porosity ϕ and water electrical conductivity σ_w values were taken from their works.

Sample	ϕ (-)	σ_w (S m^{-1})	Proposed model parameters					$NMSE$
			a (-)	c (-)	τ (-)	S_r (-)	σ_s (S m^{-1})	
Sandy loam	0.40	0.565	0.59	0.84	1.40	0.100	10.0×10^{-4}	0.0167
Sand	0.45	0.058	0.66	0.71	1.36	0.056	2.00×10^{-4}	0.0280
Mica particles	0.77	0.510	0.78	0.87	1.12	0.387	1.80×10^{-4}	0.3430
Loam	0.44	0.072	0.55	0.65	1.54	0.028	0.45×10^{-4}	0.3127

Table 2: Fitted Waxman and Smits parameter values to estimate the electrical conductivity for experimental data. The porosity ϕ and water electrical conductivity σ_w values are the values listed in Table 1.

Sample	n (-)	m (-)	σ_s^{WS} (S m^{-1})	$NMSE$	Source
Sandy loam	1.70	1.66	32.0×10^{-4}	0.0147	Amente et al. (2000)
Sand	2.00	1.53	16.5×10^{-3}	0.0034	Inoue et al. (2000)
Mica particles	2.60	2.73	97.0×10^{-4}	0.3050	Friedman and Robinson (2002)
Loam	1.60	2.62	77.4×10^{-3}	0.3144	Doussan and Ruy (2009)

Table 3: Values of the parameters used to estimate the electrical conductivity for the experimental data from Weerts et al. (1999). The porosity ϕ and water electrical conductivity σ_w values were taken from their work.

Sample	ϕ	σ_w	Proposed model parameters				$NMSE$
	(-)	(S m^{-1})	a (-)	c (-)	τ (-)	S_r (-)	
PS9	0.41	0.48	0.72	0.62	1.23	0.17	1.16×10^{-2}
PS10	0.37	0.90	0.73	0.67	1.21	0.26	1.07×10^{-2}
PS11	0.41	1.34	0.69	0.65	1.27	0.28	2.90×10^{-2}
PS13	0.40	2.25	0.74	0.58	1.28	0.27	2.50×10^{-2}

Table 4: Values of the parameters used to estimate the electrical conductivity for the experimental data from Tartrat et al. (2019).

Sample	Proposed model parameters					$NMSE$
	a (-)	c (-)	τ (-)	S_r (-)	σ_s (S m^{-1})	
1	0.53	0.46	1.55	0.34	0.026	4.40×10^{-2}
2	0.47	0.49	1.51	0.44	0.028	4.00×10^{-2}
3	0.62	0.36	1.67	0.50	0.036	3.30×10^{-2}
4	0.58	0.40	1.50	0.47	0.039	5.50×10^{-2}
5	0.40	0.59	1.37	0.42	0.042	5.10×10^{-2}
6	0.63	0.42	1.28	0.39	0.050	5.30×10^{-2}

Table 5: Values of the parameters used to estimate the electrical conductivity for the experimental data from Saafan et al. (2023).

Sample	ϕ	Proposed model parameters				$NMSE$
	(-)	a (-)	c (-)	τ (-)	S_r (-)	
S6	0.084	0.14	0.79	1.67	0.35	3.12×10^{-2}
S9	0.076	0.13	0.71	1.42	0.31	2.06×10^{-2}
S13	0.102	0.20	0.54	1.47	0.21	3.55×10^{-2}
S14	0.074	0.17	0.65	1.62	0.26	4.05×10^{-2}
S16	0.068	0.16	0.75	1.22	0.04	1.60×10^{-2}
S18	0.078	0.15	0.60	1.28	0.27	4.23×10^{-2}

of the pore radii with time (Eq. (29)), these two properties can be estimated during dissolution by (Soldi et al., 2024):

$$\phi(t) = \phi(t_0)e^{\beta(2-D)(t-t_0)} \tag{36}$$

$$k(t) = k(t_0)e^{\beta(4-D)(t-t_0)} \tag{37}$$

where $\phi(t_0)$ and $k(t_0)$ are the porosity and permeability of the REV at the initial time t_0 of the dissolution process.

The time series that we selected to fit the model correspond to a stage of the experiment when the dissolution has been already occurring since the data at the initial and final stages are out of the hypotheses of the model. The data from the beginning of the process is disregarded due to the strong dissolution, and the data from the final stages were measured after the complete percolation and the sample which then cannot be considered as a REV. Eqs. (31), (36) and (37) are fitted using an exhaustive search method by minimizing the weighted normalized error between the calculated and measured values of σ_{sat}^{REV}, ϕ and k simultaneously. Figure 9 shows the fit of the proposed model to these petrophysical properties and the values of the fitted parameters are listed in Table 6. To estimate $\phi(t_0)$, $k(t_0)$ and $\sigma_{sat}^{REV}(t_0)$ in Eqs. (36), (37), and (31), the model also requires a R_{REV} and σ_w values for which we consider the values from Rembert et al. (2023a), $R_{REV} = 9$ mm, $\sigma_w = 1200$ µS cm^{-1} for E04 and $\sigma_w = 1000$ µS cm^{-1} for E05. Note that the evolution over time of ϕ, k, and σ_{sat}^{REV} of the experimental data can be satisfactorily reproduced by the proposed model, as shown in Fig. 9(a-b), (d-c) and (e-f) respectively. It can be observed from the values of the best fitted parameters (Table 6) that they do not change significantly between the two samples. Moreover, the fitted minimum and maximum radii are consistent with the values obtained from statistical computations on tomographic images of the samples (Rembert et al., 2023a) while the fitted dissolution rate may be slightly higher than the one calculated in Léger et al. (2022a). It is important to notice that we analyse the evolution of these macroscopic properties due to the changes in the pore geometry caused by the dissolution. Therefore, variations of other parameters during the process, such as ionic concentration of the pore water, are neglected. The experimental data used in this section from Rembert et al. (2023a) account for water electrical conductivity measured at the outlet. They observed that the electrical conductivity of carbonate samples presents a significant increase at the beginning of the dissolution followed by a gentle slope that decreases its magnitude. This fact can be related to an initial strong dissolution regime that diminishes with time since water electrical conductivity is stable over this period.

To highlight the link between the evolution of hydraulic and electrical properties during the dissolution, the permeability and electrical conductivity are plotted as functions of the porosity. Fig. 10 shows the relationship between these properties for the data sets and the proposed model. We use the fitted parameters of the proposed model from Table 6. In addition, we compare them with the most classical equation to represent permeability-porosity and electrical conductivity-porosity data, the Kozeny-Carman equation (Kozeny, 1927; Carman, 1937) and Archie (1942). Following the Kozeny-Carman equation, perme-

ability can be expressed in terms of porosity as:

$$k = p\frac{\phi^3}{(1-\phi)^2}, \tag{38}$$

where p is a fitting parameter that depends on the specific internal surface area, an empirical geometrical parameter, and the tortuosity. The best agreement between the data and the Kozeny-Carman equation is obtained for $p = 1.732 \times 10^{-12}$ ($NMSE = 6.514 \times 10^{-3}$) and $p = 2.7949 \times 10^{-12}$ ($NMSE = 7.161 \times 10^{-2}$), for E04 and E05, respectively. It can be observed that the proposed model provides better results than the Kozeny-Carman equation for both samples (see Figs. 10a and b). In fact, the $NMSE$ values for the proposed model are $NMSE = 1.595 \times 10^{-5}$ for E04 and $NMSE = 3.401 \times 10^{-3}$ for E05 which are significantly smaller than for the Kozeny-Carman equation.

The relationship between the electrical conductivity and porosity given by Archie (1942) in Eq. (2), which under fully water-saturated conditions yields:

$$\sigma = \sigma_w \phi^m, \tag{39}$$

where m is the cementation exponent. For the σ_w value, we considered the values from Rembert et al. (2023a), previously mentioned for the fitting of the proposed model. The value of this fitted parameter is $m = 2.679$ ($NMSE = 1.490 \times 10^{-2}$) and $m = 2.712$ ($NMSE = 2.390 \times 10^{-2}$), for E04 and E05, respectively. Figs. 10c and d show the comparison between the data, the proposed model, and Archie (1942). It can be seen that the model from Archie (1942) has a poor performance in reproducing the data behavior while the proposed model predicts closer values. The $NMSE$ values for the proposed model are $NMSE = 7.378 \times 10^{-5}$ for E04 and $NMSE = 1.276 \times 10^{-4}$ for E05. Note that the $NMSE$ values between the Archie (1942) and the proposed model differs between 2 and 3 orders of magnitude.

From a geometrical approach, the proposed model can represent the changes of the pore structure which results in a larger porosity, permeability, and electrical conductivity of the porous medium. The comparison with classical models shows that they cannot reproduce the variations that affect these properties of the porous media under dissolution. Therefore, the proposed analytical model represents a step forward to estimate the petrophysical properties during reactive processes.

4 Discussion and conclusions

Based on the framework of capillary tubes approach, we present an analytical model to determine the electrical conductivity of a porous medium represented by tortuous capillaries with varying aperture. The periodic fluctuations of the capillary radii follow a sinusoidal piecewise behaviour along the pore length. This pore geometry determines periodical fractions of the capillaries with pore throats and pore bodies defined by two geometrical parameters, the radial a and length c factors, which allow us to represent a wide range of pore geometries. The model has analytical closed-form expressions that

Table 6: Values of the parameters used to estimate the electrical conductivity for the experimental data from Rembert et al. (2023a).

Sample	Proposed model parameters							$NMSE$
	a (-)	c (-)	D (-)	τ (-)	R_{max} (mm)	R_{min} (mm)	$\tilde{\alpha}$ (h^{-1})	
E04	0.20	0.87	1.31	1.36	0.45	1.26×10^{-4}	0.0046	1.814×10^{-3}
E05	0.28	0.82	1.29	1.25	0.86	5.50×10^{-4}	0.0055	3.521×10^{-3}

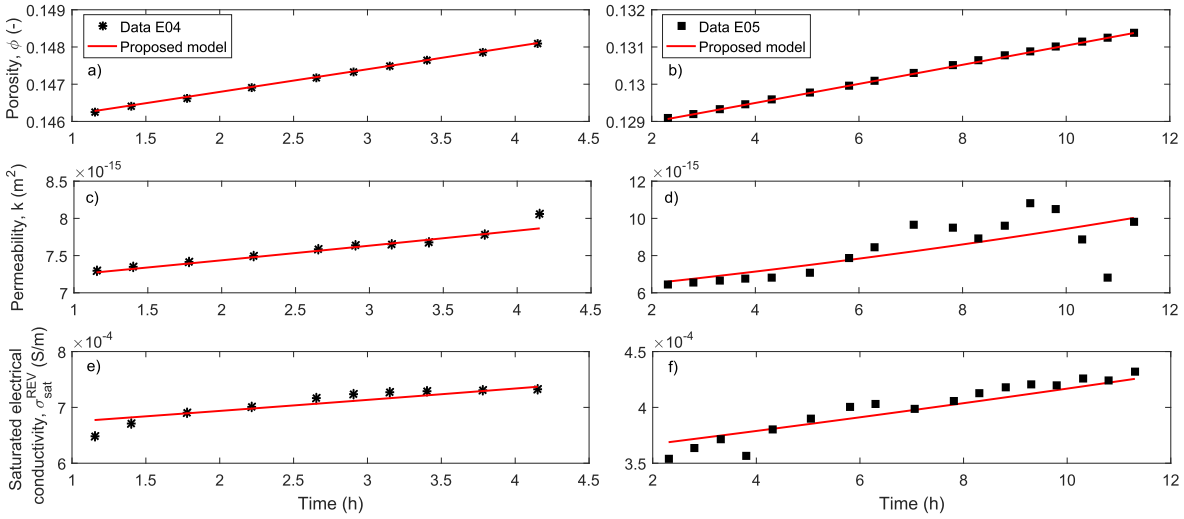

Figure 9: Model fit to the time evolution of: a-b) porosity, c-d) permeability and e-f) electrical conductivity data for samples E04 and E05 from Rembert et al. (2023a).

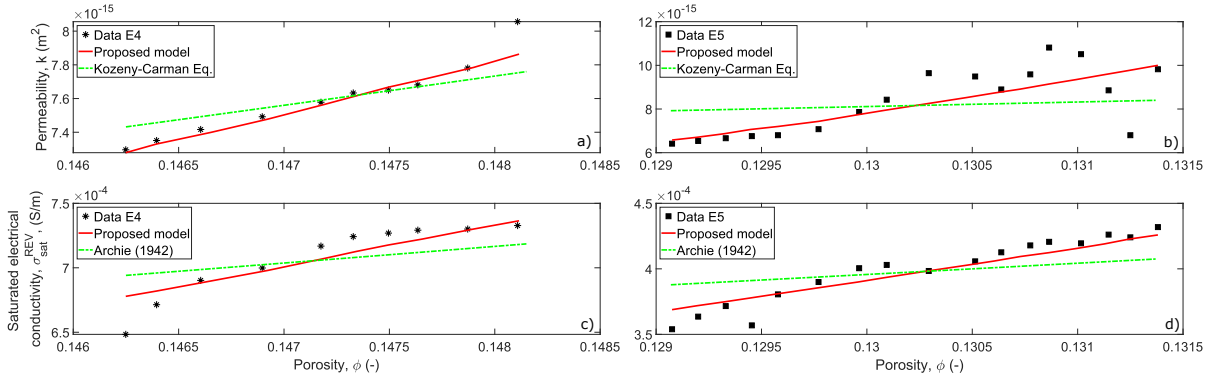

Figure 10: Comparison among the estimates of: a) and b) permeability-porosity for the proposed model and the Kozeny-Carman Equation, c) and d) electrical conductivity-porosity for the proposed model and Archie's law or samples E04 and E05 from Rembert et al. (2023a).

depend on parameters which all have a physical or geometrical meaning. In the particular case of $c = 0.5$, the proposed model is consistent with the model developed by Rembert et al. (2020) for a porous medium under water saturated conditions. In addition, the proposed model addresses partially saturated conditions and more complex processes.

The periodic throats of the pore structure allow us to introduce the hysteresis phenomenon in the relative electrical conductivity when expressed as a function of the pressure head. The resulting expressions for drainage and imbibition experiments also depend on only four independent model parameters (the fractal dimension D, the radial factor a, the minimum R_{min} and maximum R_{max} radii). Hysteretic behaviour of the electrical conductivity has been observed in experimental and numerical studies as function of saturation (e.g. Knight, 1991; Zhang et al., 2017; Maineult et al., 2018). However, from our theoretical results, hysteresis phenomena are not visible when expressed as a function of the saturation. Phenomena observed by other studies may be related to different effects, such as contact angle hysteresis, disconnection of the fluid phase (i.e., snap off), or film flow (e.g. Jury et al., 1991; Blunt et al., 2002; Spiteri et al., 2008).

In our model, the reactivity of the porous medium is introduced by considering the variations in the structure of the capillaries. Therefore, it should be noted that the model focuses only on the geometrical changes that these processes produce on the porous medium. The proposed model is compared against experimental data of electrical conductivity, porosity, and permeability during dissolution. This comparison shows that the model is satisfactorily able to reproduce the evolution of these three petrophysical properties with time simultaneously.

The performance of our model to estimate electrical conductivity is tested against different sets of experimental data. The proposed relationship between the relative electrical conductivity and effective saturation can fairly reproduce the data from different soil textures and a packing of mica particles. Moreover, when estimating the electrical conductivity for several samples of a same type of soil, the fitting parameter values vary in a narrow range for each soil. For the loamy sand case, the high values of the radial factor a and length factor c represent pores whose radii vary slightly between their constrictive and non-constrictive fractions which results in less tortuous paths due a higher connection between the fractions (e.g. Xing et al., 2021). For the illitic clay samples, the values of a are low while the tortuosity values are higher than the ones for the loamy sand. This result is consistent with this type of soil that may present more constrictive pores and complex flow paths (i.e. more tortuous) due to the packaging of its finer grains. While in the case of the sandstone samples, the significant low values of a and high values of c represent strong constrictivities of the pores (i.e. high pore radii reductions over a large length of the pores) causing that the water flow hinders and a high decrease of the permeability.

The model developed in this study represents an improvement over available models within the framework of capillary tube models by its capability to describe a wide variety of porous space geometries. In fact, it could be used to represent micropores which may have long and narrow necks (i.e. high c value and low a value) connected to larger and short pore bodies (e.g. Sun and Torres-Verdín, 2022). When compared to most

widely used models, the proposed model is consistent with the empirical model of Archie (1942) for the cases of non-constrictive capillaries, and is in good agreement with the model of Waxman and Smits (1968) for simple rock characterization. Even though the expression of these classical models to describe the electrical conductivity might be less complex, they cannot account for hysteresis effects which are of significant importance for unsaturated flow, nor for reactive phenomena that can predominate in carbonate media. On the contrary, the proposed model can represent both of these phenomena and with one set of the model parameters. This new analytical model to estimate the electrical conductivity is developed under the same framework and assumptions used previously to derive hydraulic properties (permeability, porosity). From a geometrical approach, we are capable of describing petrophysical and flow properties while accounting for their characteristic physical phenomena such as hysteresis and reactive processes. Thus, this work represents a significant step toward a unified model for many important petrophysical properties, and therefore, a way to characterize hydraulic properties of porous media from electrical measurements.

5 Notation List

Symbol	Description	Units
REV	Representative elementary volume	-
σ	Electrical conductivity	S m^{-1}
σ_w	Electrical conductivity of the electrolite	S m^{-1}
F	Formation factor	-
σ_s	Surface electrical conductivity	S m^{-1}
ϕ	Porosity	-
S_w	Water saturation	-
n, m	Archie's saturation and cementation factors, respectively	-
R	Radius of a circular tube	m
l	Pore length	m
τ	Tortuosity	-
a	Radial factor of the constrictivity	-
c	Length factor of the constrictivity	-
λ	Wavelength	m
$r(x)$	Pore radius variation along the longitudinal variable x	m
R_{REV}	REV radius	m
R_{min}, R_{max}	Minimum and maximum pore radii, respectively	m
$N(R)$	Number of pores of radius equal or larger than R	-
D	Fractal dimension	-
L	REV length	m
Σ_p	Electrical conductance of a pore	S

(It continues in the following page).

Symbol	Description	Units
f	Reduction factor in a pore conductance due to the presence of constrictivities	-
σ_p	Electrical conductivity of a pore	S m^{-1}
i_p	Electric current in a pore	A
ΔV	Electrical voltage difference	V
I^{REV}	Electric current in the REV	A
σ^{REV}	Electrical conductivity of the REV	S m^{-1}
σ^{REV}_{sat}	Electrical conductivity of the total saturated REV	S m^{-1}
f_v	Reduction factor in the porosity due to the presence of constrictivities	-
f_σ	Reduction factor in σ^{REV} due to the presence of constrictivities	-
h	Pressure head	m
T_s	Surface tension	N m^{-1}
γ	Contact angle	degrees
ρ_w	Water density	kg m^{-3}
g	Gravitational acceleration	m s^{-2}
R_h	Pore radius related to pressure head h	m
R^*	Integration variable	m
σ_{rel}	Relative electrical conductivity of the REV	-
σ^d_{rel},σ^w_{rel}	Main drying and wetting relative electrical conductivity, respectively	-
h_{min}, h_{max}	Minimum and maximum pressure heads, respectively	m
S_e, S_r	Effective and residual water saturations, respectively	-
V_p	Pore volume	m^3
t	Time	h
S_p	Pore surface	m^2
α	Dissolution rate	m^3 h^{-1}
$\tilde{\alpha}$	Dissolution rate	h^{-1}
β	Dissolution factor	h^{-1}
σ_{WS}	Electrical conductivity from Waxman and Smits (1968)	S m^{-1}
k	Permeability	m^2

Acknowledgements

This research was carried out as part of M. Soldi's postdoctoral fellowship funded by the Consejo Nacional de Investigaciones Científicas y Técnicas (Argentine). The authors strongly thank the Editor Graham Sander, and the reviews of Youzheng Qi and two anonymous reviewers for their careful assessment of our work and their valuable comments and suggestions which helped to improve the manuscript.

CRediT authorship contribution statement

Mariangeles Soldi: Conceptualization, Methodology, Investigation, Formal analysis, Writing - original draft, Writing – review & editing. Flore Rembert: Investigation, Formal analysis, Methodology, Writing – review & editing. Luis Guarracino: Conceptualization, Methodology, Writing – review & editing, Investigation, Supervision. Damien Jougnot: Conceptualization, Methodology, Writing – review & editing, Investigation, Supervision.

Data availability

No original data, everything has been published before.

References

Alkattan, M., Oelkers, E.H., Dandurand, J.L., Schott, J., 1998. An experimental study of calcite and limestone dissolution rates as a function of ph from- 1 to 3 and temperature from 25 to 80 c. Chemical geology 151, 199–214.

Amente, G., Baker, J.M., Reece, C.F., 2000. Estimation of soil solution electrical conductivity from bulk soil electrical conductivity in sandy soils. Soil Science Society of America Journal 64, 1931–1939. doi:https://doi.org/10.2136/sssaj2000.6461931x.

Archie, G.E., 1942. The electrical resistivity log as an aid in determining some reservoir characteristics. Transactions of the AIME 146, 54–62.

Binley, A., Hubbard, S.S., Huisman, J.A., Revil, A., Robinson, D.A., Singha, K., Slater, L.D., 2015. The emergence of hydrogeophysics for improved understanding of subsurface processes over multiple scales. Water resources research 51, 3837–3866.

Binley, A., Kemna, A., 2005. Dc resistivity and induced polarization methods. Hydrogeophysics , 129–156.

Binley, A., Slater, L., 2020. Resistivity and induced polarization: Theory and applications to the near-surface earth. Cambridge University Press.

Blunt, M.J., Jackson, M.D., Piri, M., Valvatne, P.H., 2002. Detailed physics, predictive capabilities and macroscopic consequences for pore-network models of multiphase flow. Advances in Water Resources 25, 1069–1089.

Breede, K., Kemna, A., Esser, O., Zimmermann, E., Vereecken, H., Huisman, J., 2011. Joint measurement setup for determining spectral induced polarization and soil hydraulic properties. Vadose zone journal 10, 716–726.

Bussian, A., 1983. Electrical conductance in a porous medium. Geophysics 48, 1258–1268.

741 Cai, J., Wei, W., Hu, X., Wood, D.A., 2017. Electrical conductivity models in saturated
742 porous media: A review. Earth-Science Reviews 171, 419–433.

743 Carman, P.C., 1937. Fluid flow through granular beds. Trans. Inst. Chem. Eng. 15,
744 150–166.

745 Celia, M.A., Dahle, H.K., Hassanizadeh, S.M., 2004. Dynamic effects in capillary pressure
746 relationships for two-phase flow in porous media: insights from bundle-of-tubes models
747 and their implications, in: Developments in Water Science. Elsevier. volume 55, pp.
748 127–138.

749 Chen, X., Thanh, L.D., Luo, C., Tahmasebi, P., Cai, J., 2023. Dependence of electrical
750 conduction on pore structure in reservoir rocks from the beibuwan and pearl river mouth
751 basins: A theoretical and experimental study. Geophysics 88, MR35–MR53.

752 Cherubini, A., Garcia, B., Cerepi, A., Revil, A., 2019. Influence of co2 on the electri-
753 cal conductivity and streaming potential of carbonate rocks. Journal of Geophysical
754 Research: Solid Earth 124, 10056–10073.

755 Clennell, M.B., 1997. Tortuosity: a guide through the maze. Geological Society, London,
756 Special Publications 122, 299–344.

757 Deceuster, J., Kaufmann, O., 2012. Improving the delineation of hydrocarbon-impacted
758 soils and water through induced polarization (ip) tomographies: A field study at an
759 industrial waste land. Journal of contaminant hydrology 136, 25–42.

760 Doolittle, J.A., Brevik, E.C., 2014. The use of electromagnetic induction techniques in
761 soils studies. Geoderma 223, 33–45.

762 Doussan, C., Ruy, S., 2009. Prediction of unsaturated soil hydraulic conduc-
763 tivity with electrical conductivity. Water Resources Research 45, W10408,
764 doi:10.1029/2008WR007309.

765 Elashahab, B., Jing, X., Archer, J., 1995. Resistivity index and capillary pressure hys-
766 teresis for rock samples of different wettability characteristics, in: SPE Middle East Oil
767 and Gas Show and Conference, SPE. pp. SPE–29888.

768 Freedman, V.L., Bacon, D.H., Saripalli, K.P., Meyer, P.D., 2004. A film depositional
769 model of permeability for mineral reactions in unsaturated media. Vadose Zone Journal
770 3, 1414–1424.

771 Friedman, S.P., 2005. Soil properties influencing apparent electrical conductivity: a re-
772 view. Computers and electronics in agriculture 46, 45–70.

773 Friedman, S.P., Robinson, D.A., 2002. Particle shape characterization using angle of
774 repose measurements for predicting the effective permittivity and electrical conductivity
775 of saturated granular media. Water Resources Research 38, 18–1–18–11.

Garing, C., Gouze, P., Kassab, M., Riva, M., Guadagnini, A., 2015. Anti-correlated porosity–permeability changes during the dissolution of carbonate rocks: experimental evidences and modeling. Transport in Porous Media 107, 595–621.

Garing, C., Luquot, L., Pezard, P.A., Gouze, P., 2014. Electrical and flow properties of highly heterogeneous carbonate rocks. AAPG Bulletin 98, 49–66.

Ghanbarian-Alavijeh, B., Millán, H., Huang, G., 2011. A review of fractal, prefractal and pore-solid-fractal models for parameterizing the soil water retention curve. Canadian Journal of Soil Science 91, 1–14.

Glover, P., 2015. Geophysical properties of the near surface earth: Electrical properties. Treatise on Geophysics 11, 89–137.

Glover, P.W., 2017. A new theoretical interpretation of archie's saturation exponent. Solid Earth 8, 805–816.

Guarracino, L., 2006. A fractal constitutive model for unsaturated flow in fractured hard rocks. Journal of Hydrology 324, 154–162.

Guarracino, L., Quintana, F., 2009. A constitutive model for water flow in unsaturated fractured rocks. Hydrological Processes: An International Journal 23, 697–701.

Guarracino, L., Rötting, T., Carrera, J., 2014. A fractal model to describe the evolution of multiphase flow properties during mineral dissolution. Advances in water resources 67, 78–86.

Heberling, F., Klačić, T., Raiteri, P., Gale, J.D., Eng, P.J., Stubbs, J.E., Gil-Díaz, T., Begović, T., Lützenkirchen, J., 2021. Structure and surface complexation at the calcite (104)–water interface. Environmental science & technology 55, 12403–12413.

Hem, J.D., Minear, R., 2012. Conductance: a collective measure of dissolved ions. Water analysis. Inorganic species 1, 137–161.

Hermans, T., Goderniaux, P., Jougnot, D., Fleckenstein, J.H., Brunner, P., Nguyen, F., Linde, N., Huisman, J.A., Bour, O., Lopez Alvis, J., et al., 2023. Advancing measurements and representations of subsurface heterogeneity and dynamic processes: towards 4d hydrogeology. Hydrology and Earth System Sciences 27, 255–287.

Herrick, D.C., Kennedy, W.D., 1994. Electrical efficiency; a pore geometric theory for interpreting the electrical properties of reservoir rocks. Geophysics 59, 918–927.

Holzer, L., Marmet, P., Fingerle, M., Wiegmann, A., Neumann, M., Schmidt, V., 2023. Tortuosity and microstructure effects in porous media: classical theories, empirical data and modern methods. Springer Nature.

Hunter, R., 1981. Zeta potential in colloid science: Principles and applications. New York, USA .

Inoue, M., Šimůnek, J., Shiozawa, S., Hopmans, J., 2000. Simultaneous estimation of soil hydraulic and solute transport parameters from transient infiltration experiments. Advances in water resources 23, 677–688.

Izumoto, S., Huisman, J.A., Wu, Y., Vereecken, H., 2020. Effect of solute concentration on the spectral induced polarization response of calcite precipitation. Geophysical journal international 220, 1187–1196.

Izumoto, S., Huisman, J.A., Zimmermann, E., Heyman, J., Gomez, F., Tabuteau, H., Laniel, R., Vereecken, H., Méheust, Y., Le Borgne, T., 2022. Pore-scale mechanisms for spectral induced polarization of calcite precipitation inferred from geo-electrical millifluidics. Environmental Science & Technology 56, 4998–5008.

Jackson, M.D., 2010. Multiphase electrokinetic coupling: Insights into the impact of fluid and charge distribution at the pore scale from a bundle of capillary tubes model. Journal of Geophysical Research: Solid Earth 115, doi:10.1029/2009JB007092.

Jougnot, D., Jiménez-Martínez, J., Legendre, R., Le Borgne, T., Méheust, Y., Linde, N., 2018. Impact of small-scale saline tracer heterogeneity on electrical resistivity monitoring in fully and partially saturated porous media: Insights from geoelectrical milli-fluidic experiments. Advances in Water Resources 113, 295–309.

Jougnot, D., Linde, N., Revil, A., Doussan, C., 2012. Derivation of soil-specific streaming potential electrical parameters from hydrodynamic characteristics of partially saturated soils. Vadose Zone Journal 11, doi:10.2136/vzj2011.0086.

Jougnot, D., Mendieta, A., Leroy, P., Maineult, A., 2019. Exploring the effect of the pore size distribution on the streaming potential generation in saturated porous media, insight from pore network simulations. Journal of Geophysical Research: Solid Earth 124, 5315–5335.

Jurin, J., 1717. An account of some experiments shown before the royal society; with an enquiry into the cause of the ascent and suspension of water in capillary tubes. by james jurin, md and r. soc. s. Philosophical Transactions 30, 739–747.

Jury, W.A., Gardner, W.R., Gardner, W.H., 1991. Soil physics. John Wiley & Sons, Inc. New York .

Kaufmann, G., Dreybrodt, W., 2007. Calcite dissolution kinetics in the system caco3–h2o–co2 at high undersaturation. Geochimica et Cosmochimica Acta 71, 1398–1410.

Knight, R., 1991. Hysteresis in the electrical resistivity of partially saturated sandstones. Geophysics 56, 2139–2147.

Knight, R.J., Endres, A.L., 2005. An introduction to rock physics principles for near-surface geophysics, in: Near-surface geophysics. Society of Exploration Geophysicists, pp. 31–70.

Kozeny, J., 1927. Uber kapillare leitung der wasser in boden. Royal Academy of Science, Vienna, Proc. Class I 136, 271–306.

Laloy, E., Javaux, M., Vanclooster, M., Roisin, C., Bielders, C., 2011. Electrical resistivity in a loamy soil: Identification of the appropriate pedo-electrical model. Vadose Zone Journal 10, 1023–1033.

Leger, M., Luquot, L., 2021. Importance of microstructure in carbonate rocks: laboratory and 3d-imaging petrophysical characterization. Applied Sciences 11, 3784.

Léger, M., Luquot, L., Roubinet, D., 2022a. Role of mineralogical, structural and hydrodynamic rock properties in conduits formation in three distinct carbonate rock types. Chemical Geology 607, 121008.

Léger, M., Roubinet, D., Jamet, M., Luquot, L., 2022b. Impact of hydro-chemical conditions on structural and hydro-mechanical properties of chalk samples during dissolution experiments. Chemical Geology 594, 120763.

Leroy, P., Li, S., Jougnot, D., Revil, A., Wu, Y., 2017. Modelling the evolution of complex conductivity during calcite precipitation on glass beads. Geophysical Journal International 209, 123–140.

Leroy, P., Revil, A., 2004. A triple-layer model of the surface electrochemical properties of clay minerals. Journal of Colloid and interface Science 270, 371–380.

Lévy, L., Gibert, B., Sigmundsson, F., Flóvenz, O.G., Hersir, G., Briole, P., Pezard, P., 2018. The role of smectites in the electrical conductivity of active hydrothermal systems: electrical properties of core samples from krafla volcano, iceland. Geophysical Journal International 215, 1558–1582.

Liang, M., Yang, S., Yu, B., 2014. A fractal streaming current model for charged microscale porous media. Journal of Electrostatics 72, 441–446.

Linde, N., Binley, A., Tryggvason, A., Pedersen, L.B., Revil, A., 2006. Improved hydrogeophysical characterization using joint inversion of cross-hole electrical resistance and ground-penetrating radar traveltime data. Water Resources Research 42.

Liu, Z., Yuan, D., Dreybrodt, W., 2005. Comparative study of dissolution rate-determining mechanisms of limestone and dolomite. Environmental Geology 49, 274–279.

Loiseau, B., Carrière, S.D., Jougnot, D., Singha, K., Mary, B., Delpierre, N., Guérin, R., Martin-StPaul, N.K., 2023. The geophysical toolbox applied to forest ecosystems–a review. Science of the Total Environment , 165503.

Longeron, D., Argaud, M., Feraud, J.P., 1989. Effect of overburden pressure and the nature and microscopic distribution of fluids on electrical properties of rock samples. SPE Formation Evaluation 4, 194–202.

Luo, H., Jougnot, D., Jost, A., Teng, J., Thanh, L.D., 2023. A capillary bundle model for the electrical conductivity of saturated frozen porous media. Journal of Geophysical Research: Solid Earth , e2022JB025254.

Maineult, A., Jougnot, D., Revil, A., 2018. Variations of petrophysical properties and spectral induced polarization in response to drainage and imbibition: a study on a correlated random tube network. Geophysical Journal International 212, 1398–1411.

Mohammadmoradi, P., Behrang, A., Kantzas, A., 2016. Effective thermal and electrical conductivity of two-phase saturated porous media, in: SPE Canada Heavy Oil Conference, SPE. p. D021S010R004.

Mualem, Y., Friedman, S., 1991. Theoretical prediction of electrical conductivity in saturated and unsaturated soil. Water Resources Research 27, 2771–2777.

Müller-Huber, E., Schön, J., Börner, F., 2015. The effect of a variable pore radius on formation resistivity factor. Journal of Applied Geophysics 116, 173–179.

Niu, Q., Zhang, C., 2019. Permeability prediction in rocks experiencing mineral precipitation and dissolution: a numerical study. Water Resources Research 55, 3107–3121.

Noiriel, C., Gouze, P., Bernard, D., 2004. Investigation of porosity and permeability effects from microstructure changes during limestone dissolution. Geophysical research letters 31.

Olabode, O.P., San, L.H., Ramli, M.H., 2020. Analysis of geotechnical-assisted 2-d electrical resistivity tomography monitoring of slope instability in residual soil of weathered granitic basement. Frontiers in Earth Science 8, 580230.

Olsen, P.A., 2011. Coarse-scale resistivity for saturation estimation in heterogeneous reservoirs based on archie's formula. Geophysics 76, E35–E43.

Patnode, H., Wyllie, M., 1950. The presence of conductive solids in reservoir rocks as a factor in electric log interpretation. Journal of petroleum technology 2, 47–52.

Qi, Y., Wu, Y., 2022. Electrical conductivity of clayey rocks and soils: A non-linear model. Geophysical Research Letters 49, e2021GL097408.

Qi, Y., Wu, Y., 2024. Induced polarization of clayey rocks and soils: Non-linear complex conductivity models. Journal of Geophysical Research: Solid Earth 129, e2023JB028405.

Regnet, J., David, C., Robion, P., Menéndez, B., 2019. Microstructures and physical properties in carbonate rocks: A comprehensive review. Marine and Petroleum Geology 103, 366–376.

916 Rembert, F., Jougnot, D., Guarracino, L., 2020. A fractal model for the electrical con-
917 ductivity of water-saturated porous media during mineral precipitation-dissolution pro-
918 cesses. Advances in Water Resources 145, 103742.

919 Rembert, F., Jougnot, D., Luquot, L., Guérin, R., 2022. Interpreting self-potential signal
920 during reactive transport: application to calcite dissolution and precipitation. Water
921 14, 1632.

922 Rembert, F., Léger, M., Jougnot, D., Luquot, L., 2023a. Geoelectrical and hydro-chemical
923 monitoring of karst formation at the laboratory scale. Hydrology and Earth System
924 Sciences 27, 417–430.

925 Rembert, F., Stolz, A., Soulaine, C., Roman, S., 2023b. A microfluidic chip for geoelec-
926 trical monitoring of critical zone processes. Lab on a Chip 23, 3433–3442.

927 Revil, A., 2013a. Effective conductivity and permittivity of unsaturated porous materials
928 in the frequency range 1 mhz–1ghz. Water resources research 49, 306–327.

929 Revil, A., 2013b. On charge accumulation in heterogeneous porous rocks under the influ-
930 ence of an external electric field. Geophysics 78, D271–D291.

931 Revil, A., Karaoulis, M., Johnson, T., Kemna, A., 2012. Some low-frequency electrical
932 methods for subsurface characterization and monitoring in hydrogeology. Hydrogeology
933 Journal 20, 617.

934 Saafan, M., Mohyaldinn, M., Elraies, K., 2023. Obtaining capillary pressure curves from
935 resistivity measurements in low-permeability sandstone. Geoenergy Science and Engi-
936 neering 221, 111297.

937 Saneiyan, S., Ntarlagiannis, D., Ohan, J., Lee, J., Colwell, F., Burns, S., 2019. Induced
938 polarization as a monitoring tool for in-situ microbial induced carbonate precipitation
939 (micp) processes. Ecological engineering 127, 36–47.

940 Schechter, R., Gidley, J., 1969. The change in pore size distribution from surface reactions
941 in porous media. AIChE Journal 15, 339–350.

942 Schön, J.H., 2015. Physical properties of rocks: Fundamentals and principles of petro-
943 physics. Elsevier.

944 Schwartz, N., Furman, A., 2012. Spectral induced polarization signature of soil con-
945 taminated by organic pollutant: Experiment and modeling. Journal of Geophysical
946 Research: Solid Earth 117.

947 Sen, P., Scala, C., Cohen, M., 1981. A self-similar model for sedimentary rocks with
948 application to the dielectric constant of fused glass beads. Geophysics 46, 781–795.

949 Singha, K., Day-Lewis, F.D., Lane Jr, J.W., 2007. Geoelectrical evidence of bicontinuum
950 transport in groundwater. Geophysical Research Letters 34.

Soldi, M., Guarracino, L., Jougnot, D., 2017. A simple hysteretic constitutive model for unsaturated flow. Transport in Porous Media 120, 271–285.

Soldi, M., Guarracino, L., Jougnot, D., 2022. The effect of pore geometry in constitutive hysteretic models for unsaturated water flow. Environmental Fluid Mechanics 22, 1283–1305.

Soldi, M., Guarracino, L., Jougnot, D., 2024. Predicting streaming potential in reactive media: the role of pore geometry during dissolution and precipitation. Geophysical Journal International 236, 967–978. doi:https://doi.org/10.1093/gji/ggad457.

Spiteri, E.J., Juanes, R., Blunt, M.J., Orr, F.M., et al., 2008. A new model of trapping and relative permeability hysteresis for all wettability characteristics. Spe Journal 13, 277–288.

Sun, Z., Mehmani, A., Torres-Verdín, C., 2021. Pore-scale investigation of the electrical resistivity of saturated porous media: flow patterns and porosity efficiency. Journal of Geophysical Research: Solid Earth 126, e2021JB022608.

Sun, Z., Torres-Verdín, C., 2022. The role of pore-shape and pore-space heterogeneity in non-archie behavior of resistivity index curves. Journal of Geophysical Research: Solid Earth 127, e2022JB024792.

Tartrat, T., Revil, A., Abdulsamad, F., Ghorbani, A., Jougnot, D., Coperey, A., Yven, B., de la Vaissiere, R., 2019. Induced polarization response of porous media with metallic particles—part 10: Influence of desiccation. Geophysics 84, E357–E375.

Thanh, L.D., Jougnot, D., Van Do, P., Tuyen, V.P., Ca, N.X., Hien, N.T., 2020. A physically based model for the electrical conductivity of partially saturated porous media. Geophysical Journal International 223, 993–1006.

Thanh, L.D., Jougnot, D., Van Do, P., Van Nghia A, N., 2019. A physically based model for the electrical conductivity of water-saturated porous media. Geophysical Journal International 219, 866–876.

Thanh, L.D., Van Nghia, N., Van Do, P., Du, P.T., Jougnot, D., 2023. A unified model for the permeability, electrical conductivity and streaming potential coupling coefficient in variably saturated fractured media. Geophysical Prospecting 71, 279–291.

Tyler, S.W., Wheatcraft, S.W., 1990. Fractal processes in soil water retention. Water Resources Research 26, 1047–1054.

Verwer, K., Eberli, G.P., Weger, R.J., 2011. Effect of pore structure on electrical resistivity in carbonates. AAPG bulletin 95, 175–190.

Wang, K.W., Sun, J.M., Guan, J.T., Zhu, D.W., 2007. A percolation study of electrical properties of reservoir rocks. Physica A: Statistical Mechanics and its Applications 380, 19–26.

Waxman, M., Smits, L., 1968. Electrical conductivities in oil-bearing shaly sands. Society of Petroleum Engineers Journal 8, 107–122.

Weerts, A., Bouten, W., Verstraten, J., 1999. Simultaneous measurement of water retention and electrical conductivity in soils: Testing the mualem-friedman tortuosity model. Water Resources Research 35, 1781–1787.

Wicki, A., Hauck, C., 2022. Monitoring critically saturated conditions for shallow landslide occurrence using electrical resistivity tomography. Vadose Zone Journal 21, e20204.

Wilson, R.C., Freeland, R.S., Wilkerson, J.B., Yoder, R.E., 2002. Imaging the lateral migration of subsurface moisture using electromagnetic induction, in: 2002 ASAE Annual Meeting, American Society of Agricultural and Biological Engineers. p. 1.

Wu, Y., Hubbard, S., Williams, K.H., Ajo-Franklin, J., 2010. On the complex conductivity signatures of calcite precipitation. Journal of Geophysical Research: Biogeosciences 115.

Wyllie, M., Southwick, P., 1954. An experimental investigation of the sp and resistivity phenomena in dirty sands. Journal of Petroleum Technology 6, 44–57.

Xing, X., Yu, M., Xia, T., Ma, L., 2021. Interactions between water flow and microplastics in silt loam and loamy sand. Soil Science Society of America Journal 85, 1956–1962.

Yu, B., 2008. Analysis of flow in fractal porous media. Applied Mechanics Reviews 61, 050801.

Yu, B., Li, J., Li, Z., Zou, M., 2003. Permeabilities of unsaturated fractal porous media. International journal of multiphase flow 29, 1625–1642.

Zhang, J., Vinogradov, J., Leinov, E., Jackson, M., 2017. Streaming potential during drainage and imbibition. Journal of Geophysical Research: Solid Earth 122, 4413–4435.

Zhu, Q., Lin, H., Doolittle, J., 2010. Repeated electromagnetic induction surveys for determining subsurface hydrologic dynamics in an agricultural landscape. Soil Science Society of America Journal 74, 1750–1762.